

Coronal magnetic fields inferred from IR wavelength and comparison with EUV observations

Y. Liu

Yunnan Astronomical Observatory, National Astronomical Observatories, Kunming 650011, China
Institute for Astronomy, University of Hawaii, 34 Ohia Ku Street, Pukalani, HI 96768, USA

Received: 23 May 2009 – Revised: 20 June 2009 – Accepted: 2 July 2009 – Published: 13 July 2009

Abstract. Spectropolarimetry using IR wavelength of 1075 nm has been proved to be a powerful tool for directly mapping solar coronal magnetic fields including transverse component directions and line-of-sight component intensities. Solar tomography, or stereoscopy based on EUV observations, can supply 3-D information for some magnetic field lines in bright EUV loops. In a previous paper (Liu and Lin, 2008) the locations of the IR emission sources in the 3-D coordinate system were inferred from the comparison between the polarization data and the potential-field-source-surface (PFSS) model, for one of five west limb regions in the corona (Lin et al., 2004). The paper shows that the region with the loop system in the active region over the photospheric area with strong magnetic field intensity is the region with a dominant contribution to the observed Stokes signals. So, the inversion of the measured Stokes parameters could be done assuming that most of the signals come from a relatively thin layer over the area with a large photospheric magnetic field strength. Here, the five limb coronal regions are studied together in order to study the spatial correlation between the bright EUV loop features and the inferred IR emission sources. It is found that, for the coronal regions above the stronger photospheric magnetic fields, the locations of the IR emission sources are closer to or more consistent with the bright EUV loop locations than those above weaker photospheric fields. This result suggests that the structures of the coronal magnetic fields observed at IR and EUV wavelengths may be different when weak magnetic fields present there.

Keywords. Solar physics, astrophysics, and astronomy (Corona and transition region; Magnetic fields)

1 Introduction

The solar coronal magnetic fields play a dominant role in the coronal plasmas distribution and dynamics. During the last decades, a few useful methods have been developed based on model assumptions for radio observations to derive coronal magnetic field strength (e.g. Stelzried et al., 1970; Patzold et al., 1987; Gary and Hurford, 1994; Alissandrakis and Drago, 1995; Brosius et al., 1997; Lee et al., 1999; Borovik et al., 1999; Aurass et al., 2005); or based on the scattering polarization of coronal emission lines (CELs) to map coronal magnetic field directions (Mickey, 1973; Querfeld and Smartt, 1984; Arnaud and Newkirk, 1987; Lin et al., 1998). Some valuable progresses have been made recently which use the strong infrared Fe XIII 1075 nm CEL for Zeeman splitting observations (Kuhn, 1995; Lin et al., 2000, 2004). Based on the Zeeman effect, the coronal flux density can be deduced with a high sensitivity of about 1 G with the current technologies (Casini and Judge, 1999; Lin and Casini, 2000). Penn et al. (2004) studied the noise sources in coronagraphic magnetic field strength measurements. Tomczyk and colleagues have found the direct evidence of Alfvén waves in the corona with their new instrument CoMP (Tomczyk et al., 2007, 2008, 2009). The recent reviews on IR coronal magnetic field measurements and inversions can be found in Kramar et al. (2006); Liu and Lin (2009); Cargill (2009).

The imaging coronal spectropolarimeter named SOLARC (Solar Observatory for Limb Active Regions and Coroneae) had been installed on Haleakala (Kuhn et al., 2003). A line-of-sight (LOS) coronal magnetogram was shown by Lin et al. (2004) as one of the first results taken by SOLARC. What coronal magnetic field information can be obtained from the new IR data is a cardinal question that needs to be answered. Judge (2007) has studied theoretical aspects of this problem, pointing to the determination of the atomic alignment as a significant observational challenge. Liu and Lin (2008) studied in detail a limb coronal region observed on 7 April 2004



Correspondence to: Y. Liu
(lyu@mail.ynao.ac.cn)

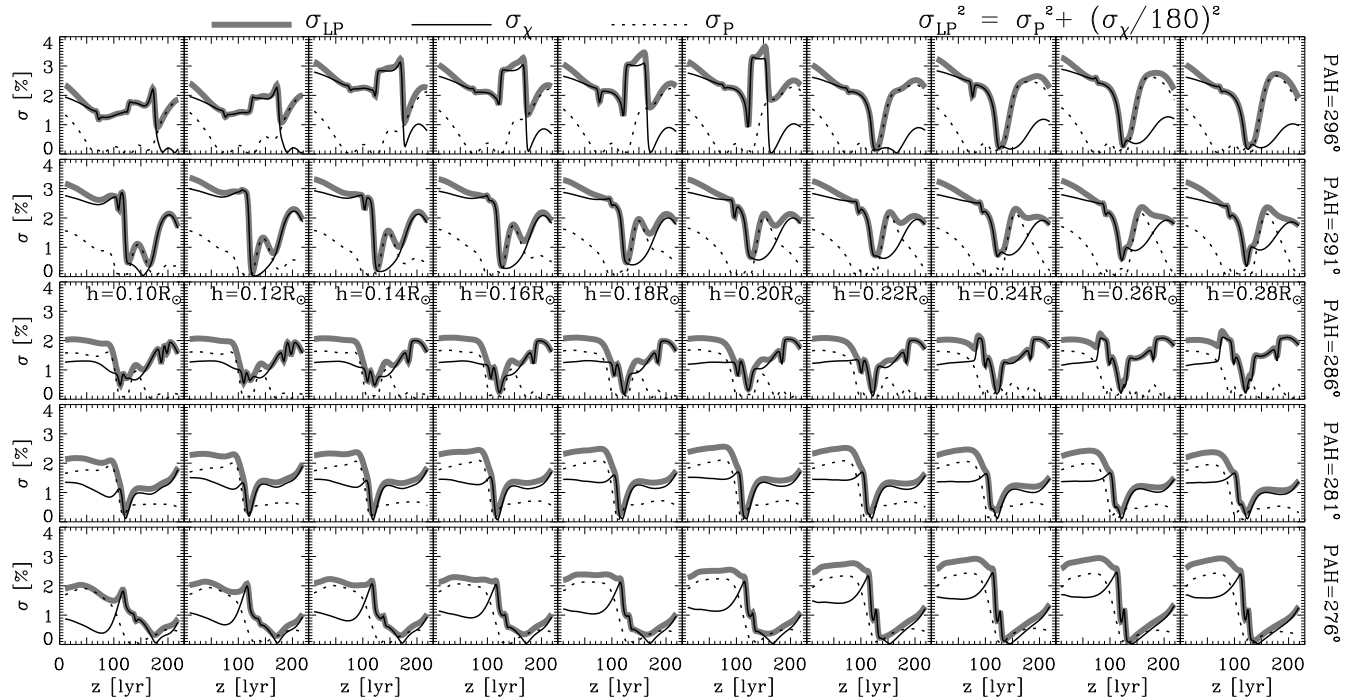


Fig. 1. Error profiles for the five coronal regions with PAH at 296, 291, 286, 281, and 276 degrees, respectively. The location (z or $\text{layer}_{\text{best}}$) of the minimum error in a σ_{LP} profile is thought to be the dominant IR coronal “emission source” along the LOS. For convenience, only the 1st–10th fibers at the 3rd row of the fiber head array (16×8) are shown for each coronal region. Most profiles (thick gray lines; σ_{LP}) show a clear minimum value between layer 120 (above a sunspot) and layer 155 (the plane of the sky through the sun center). σ_P and σ_χ are the difference between the theoretical results and SOLARC observations for linear polarization degree and azimuth angle, respectively. Note, $1 \text{ lyr} = 4.5 \text{ Mm}$.

by comparing the observed circular and linear polarizations with the synthesized maps based on the potential field model. The comparison procedure was accomplished point by point along the LOS in the datacube. The best consistence for both linear and circular polarizations was found at the layer in the corona above a sunspot near the solar limb, indicating that local coronal magnetic fields may be revealed from the IR polarization data with the proper coronal magnetic field inversion method.

In this paper, we use the linear polarization data by SOLARC to study the five limb coronal regions together. We solve the single points along each LOS using methods developed by Liu and Lin (2008), by minimizing differences between observed and computed linear polarizations taken from a potential field extrapolation. The derived points from IR data are compared with EUV images of Fe XII.

2 Results

The five west limb coronal regions had been shown in Fig. 2 of Lin et al. (2004) with PAH (i.e., the Position Angle in the Heliocentric coordinate system) of 296, 291, 286, 281, and 276 degrees, separately. The coordinate system and the pa-

rameters used in this paper are the same as in Liu and Lin (2008) for IR coronal emission sources inference from the SOLARC spectropolarimetric data. In the coordinate system, the x -axis points to the geographic west direction and the z -axis is parallel to the LOS. Different from the last paper which focused on one coronal region with both circular and linear polarization observations, in this study we apply the optimized procedure to all five coronal regions with linear polarization data available. The profile difference (rms error; σ) for each fiber point is a function of the coordinate z along the sight line. The differences represent the deviations between the theoretical and the observational polarizations. σ_P is for linear polarization amplitude, σ_χ is for azimuthal angle and σ_{LP} is the combination of the two, i.e., $\sigma_{LP}^2 = \sigma_P^2 + \sigma_\chi^2$.

Similar to results of the region PAH 286 (Liu and Lin, 2008), the profiles of σ_{LP} vs. z in the other four regions also show a clear dip. As a typical comparison, Fig. 1 shows the σ_{LP} profiles for each region at a same fiber row. Such a common feature for different coronal regions is worthy of study. Based on the results of Liu and Lin (2008), in which the identical peak/valley locations were noticed for different profiles (σ_{LP} , σ_χ , σ_P , coronal electron density, magnetic

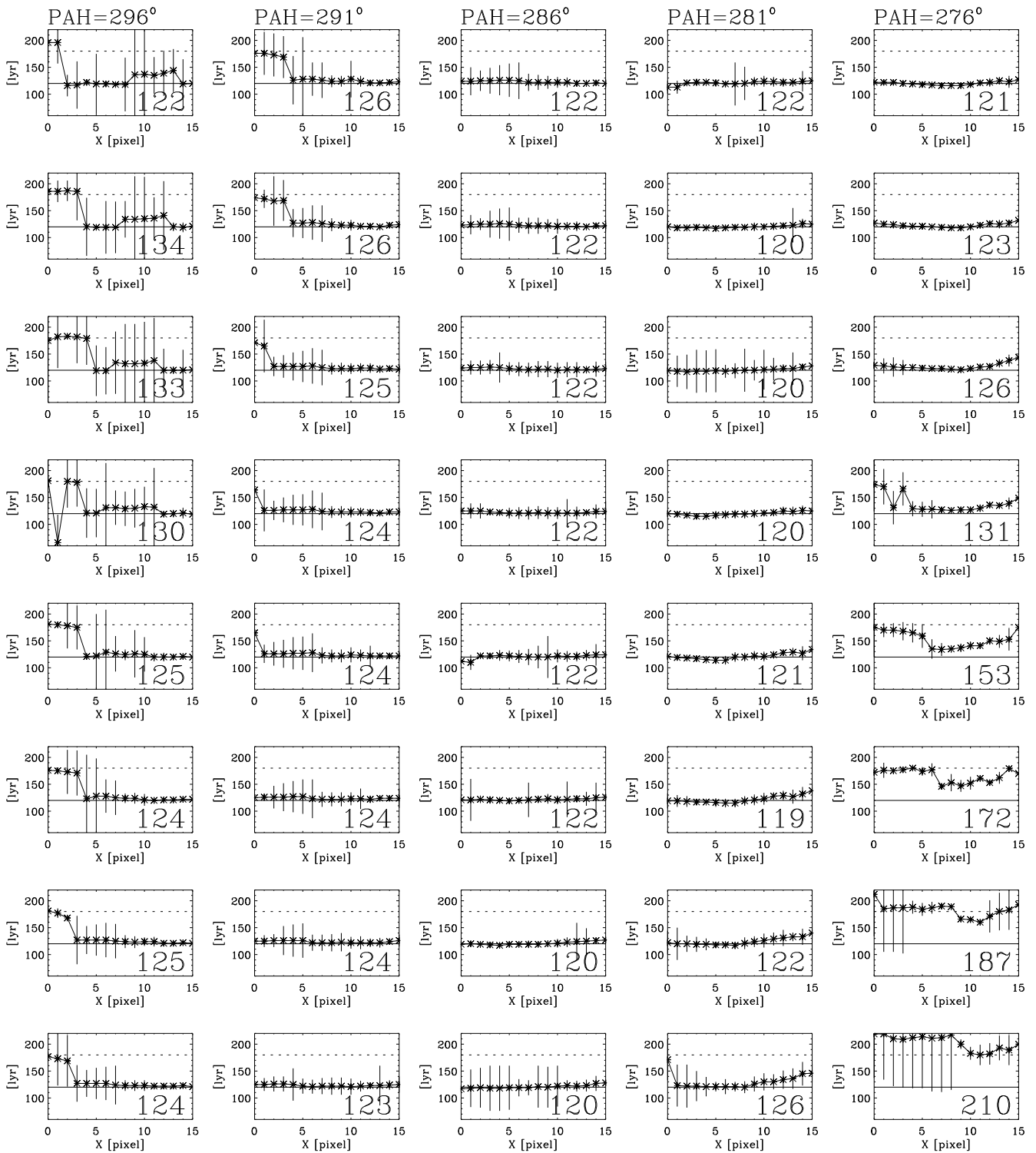


Fig. 2. $layer_{best}$, i.e., IR emission source locations inferred by the method of Liu and Lin (2008), as a function of position (in fiber head array) for the five coronal regions. The rows in each column represent the eight rows of the fiber head array (16×8). The error bar is defined to be the difference between σ_p and σ_χ (Fig. 1). The median value of the $layer_{best}$ in a row is shown as a number at the lower right corner of each box.

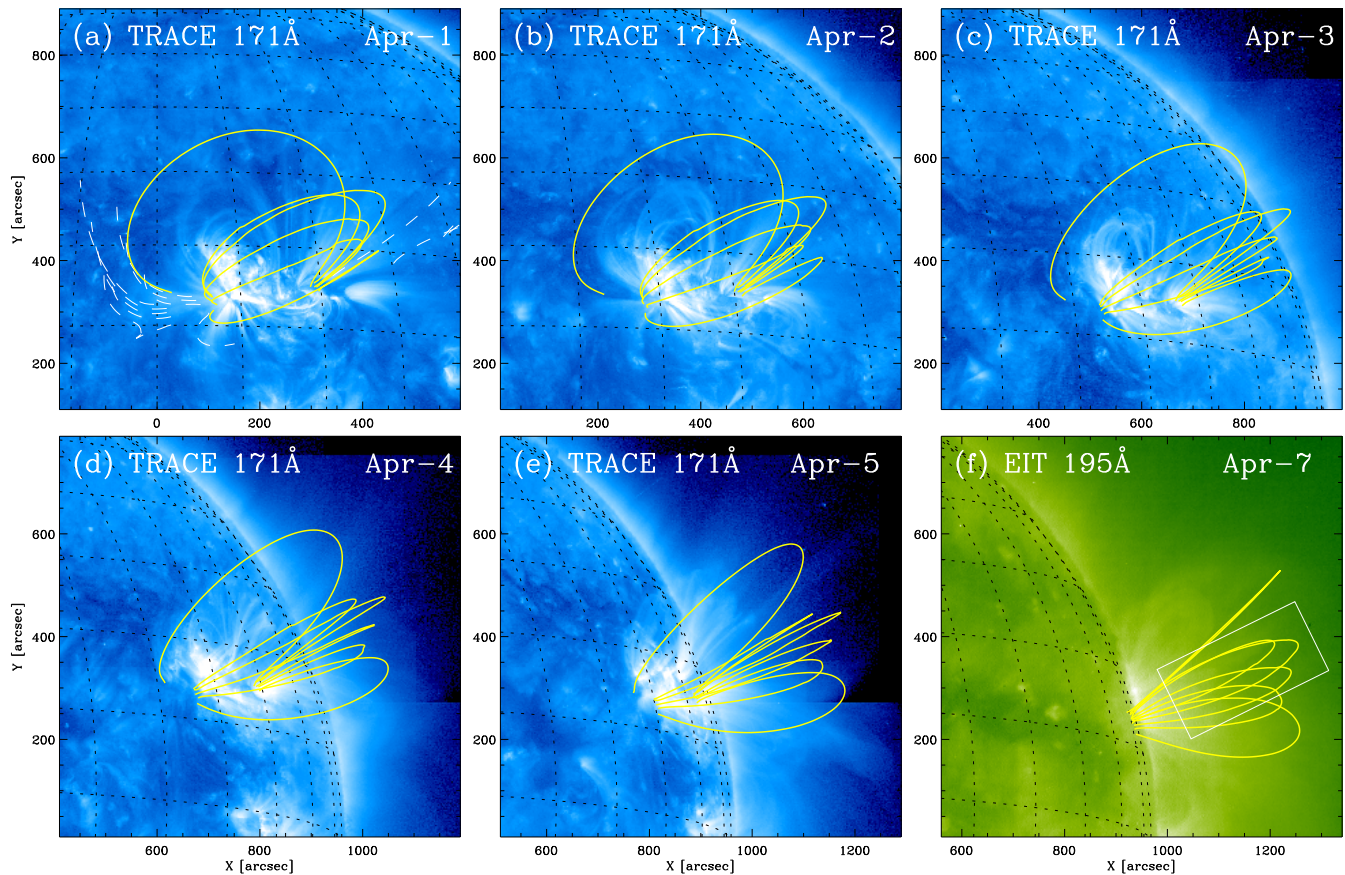


Fig. 3. The active region configurations seen in the EUV wavelengths with solar rotation in one week. The yellow lines are made by the PFSS method extrapolation and they are overlaid on the EUV images for configurational comparison. The white rectangle region in the last frame (7 April) shows the field of view of the SOLARC observation.

field energy density and Stokes V reversal signals), we deduce that this identical spatial relation was a result caused by the same coronal region above a sunspot with dominant emission sources which contributed much more photon flux for our IR observations than the other coronal fields did along the LOS. With this method, we may localize a position along the LOS with a very valuable contribution to the measured Stokes components. The error of the deduced location z in the method can be defined to be the difference between σ_χ and σ_p . The smaller the difference is, the smaller the error for the deduced z .

Figure 2 shows the z values (in unit of layer, i.e., lyr ; $Layer_{best}$) with error bars by the method for each fiber data in all five coronal regions. Note that the first layer ($lyr = 1$) and the last layer ($lyr = 205$) are located 720 Mm in front and 250 Mm behind the plane of the sky containing the sun center. The separation between the layers is about 4.5 Mm. It can be seen that most derived IR emission sources are mainly distributed at around $z = 120$ where the sunspot region NOAA 10582 is located near the solar limb on the photosphere.

If we presume that the basic coronal structures in EUV wavelengths be kept stable and the same during the days before the solar limb SOLARC observation, it would be interesting to compare the inferred IR emission sources with the EUV bright features. The assumption is supported by the fact that very low solar activities seen in the sunspot region NOAA 10582 for a week before it was rotated to the west limb. Figure 3 shows the active region with its EUV configuration kept almost the same throughout the week. The yellow lines are produced using the extrapolation based on the PFSS model (Liu and Zhang, 2002), and the white rectangle is the field of view of the SOLARC observations on 7 April 2004. We rotate back the 3-D coordinates of the IR emission sources to the date when the sunspot region was on the solar disk center. The new 2-D coordinates (x, y) of the IR emission sources can then be overlaid directly on the EUV images for comparison. Figure 4 shows the results for the five coronal regions from the top frame to the bottom frame, respectively. The IR emission sources of the two northern regions (PAH 296 and 291) are found to be distributed in two clusters, but they appear to be more dispersed for the region

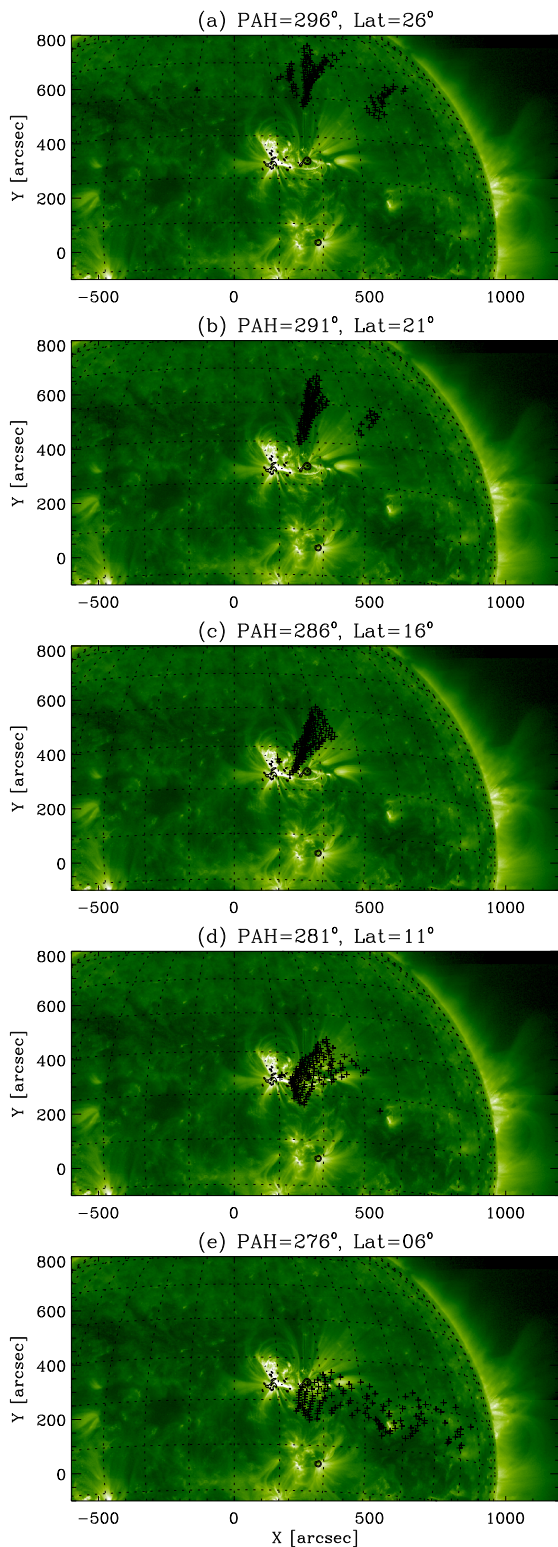


Fig. 4. Two-dimensional spatial relation between $layer_{best}$ (IR emission sources inferred by Liu and Lin's method; marked by black plus signs) and the EUV bright features on disk. The magnetic field contours denote the sunspots positions on the photosphere.

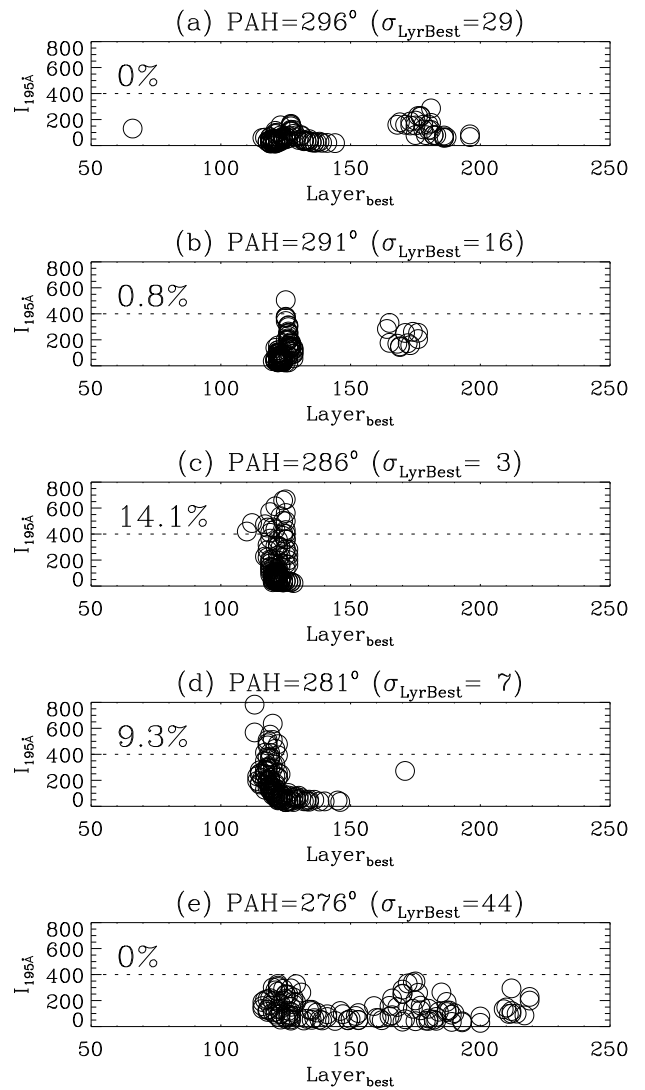


Fig. 5. Relation between $layer_{best}$ (IR emission sources locations by Liu and Lin's method; with open circles) and the corresponding EUV brightness at limb. It can be concluded, for one coronal region, that the larger the percentage of bright EUV points ($I > 0.5I_{max}$) it has, the more compact the distribution of the IR emission sources appears (parameterized by $\sigma_{LyrBest}$).

of PAH 296 which is the furthest coronal region from the strong sunspot fields (shown with contours). The IR emission sources of the two coronal regions of PAH 286 and 281 are well distributed in more compact layers than the two northern ones. They extend in one dense cluster and they are found to cover the right parts of the EUV bright loops originating from the north active region NOAA 10582. In contrast, the scatters of the IR emission sources in the coronal region of PAH 276 appear to be much more diffused than all of the other coronal regions. From the SOLARC limb observation on 7 April, this region was just located at the top of a bundle

of north-south directed transequatorial loops (Fig. 2 in Lin et al., 2004). If the results by the polarization inversion method correctly reveal the true IR emission source locations, then this transequatorial loop system should be optically thin for the IR line formation and the loop system can be formed by many magnetic field lines in wide distributions in the corona.

3 Discussion and conclusion

We apply the optimized Liu and Lin's method built in the paper of Liu and Lin (2008) for locating observed coronal magnetic fields from IR linear polarization data to all five coronal regions observed on 7 April 2004. The idea of this method is different from the traditional ways which take the corona emission as optically thin for IR observations along sight line (e.g. Judge et al., 2006). However, the idea of trying to use one point along each LOS as a starting point for coronal magnetic field diagnosis has been present for many years (Querfeld, 1982; Judge, 2003). Kramar and Inhester (2007) showed the possibility of inversion of the coronal magnetic field from IR polarimetric observations using the Hanle effect.

In the previous paper (Liu and Lin, 2008), we had found the clear single valley shown in the LOS profiles of inferred IR source regions for one coronal region with full Stokes parameters taken. The smallest deviation between the theoretical and the observational polarization maps indicate the best consistency between them, thus the valley (minimum) locations can be thought to be the dominant IR emission source places. Based on this idea, we infer the source regions for IR emission line for all the five regions with the same method. We find that most of their profiles also show only one conspicuous dip in the long integration path along the sight line. Therefore, the only dominant emission source can be decided on from the data with this method. Most of the IR emission sources are distributed in clusters. Interestingly, when we overlay the IR emission sources inferred by Liu and Lin's method on the EUV image of one week before the limb observations, we find that the correspondence between the sources and the bright EUV features has a close relationship to strong magnetic field on the photosphere. The closer to strong photospheric field for the coronal region, the more compact the distribution of the IR emission sources. The IR emission source locations of the two regions close to the sunspot have the best correspondence to the bright EUV loop features (Fig. 4c–d). However, for the coronal region at the top of a large transequatorial loop system, its IR emission sources appear rather diffusely, suggesting a much wider IR contribution function for the formation of the 1075 nm line in it. From the five regions studied above, it is important to point out that the current SOLARC observations can reveal local magnetic field configuration in the corona only under some favorable conditions, i.e., we should take the IR polarization observations in the low coronal regions close to

strong photospheric fields at the limb. In this sense, the emissions from the unevenly distributed IR source regions along the LOS are expected to be contributed dominantly from the denser plasma above the strong photospheric fields. These magnetic field observations for local corona are very important for the direct testing of various solar eruption theories like flares and coronal mass ejections. For this testing purpose, however, we should use a non-linear force free model in our method because the potential field model indicates no free magnetic energy in the corona for the eruptions.

Practically, we usually operate SOLARC to observe the limb coronal regions with strong EUV 195 Å emissions for routine IR polarization measurements. The results of this paper have confirmed the advantage by taking SOLARC observations with the reference from EUV wavelength images to obtain useful information for the study of local coronal magnetic fields. Figure 5 shows the plots of EUV intensity vs. the inferred IR sources locations ($Layer_{best}$) for the five coronal regions. The EUV data have been processed with the standard solar software procedures. A general tendency can be seen: the higher the percentage of EUV bright points for a field of view, the more concentrated the distributions of the IR emission sources. In the next step, we plan to compare the inferred 3-D IR source regions with the 3-D structure of the bright EUV features with the help of coronal tomography technology or the 3-D STEREO EUV data.

Acknowledgements. I thank Phil Judge and another anonymous referee for their helpful comments on the manuscript. This work has been supported by the National Natural Science Foundation of China 10843010.

Topical Editor R. Forsyth thanks P. Judge and another anonymous referee for their help in evaluating this paper.

References

- Alissandrakis, C. A. and Drago, F. C.: Coronal magnetic fields from Faraday rotation observations, *Solar Phys.*, 160, 171–179, 1995.
- Arnaud, J. and Newkirk, G., Jr.: Mean properties of the polarization of the Fe XIII 10747 Å coronal emission line, *Astron. Astrophys.*, 178, 263–268, 1987.
- Aurass, H., Rausche, G., Mann, G., and Hofmann, A.: Fiber bursts as 3D coronal magnetic field probe in postflare loops, *Astron. Astrophys.*, 435, 1137–1148, 2005.
- Borovik, V. N., Medar, V. G., and Korzhavin, A. N.: First measurements of the magnetic field in a coronal hole from RATAN-600 radio observations of the Sun, *Astron. Lett.*, 25, 250–257, 1999.
- Brosius, J. W., Davila, J. M., Thomas, R. J., and White, S. M.: Coronal magnetography of a solar active region using coordinated SERTS and VLA observations, *Astrophys. J.*, 488, 488–498, 1997.
- Cargill, P. J.: Coronal Magnetism: Difficulties and Prospects, *Space Sci. Rev.*, 144, 413–421, 2009.
- Casini, R. and Judge, P. G.: Spectral lines for polarization measurements of the coronal magnetic field. II. consistent treatment of the Stokes vector for magnetic-dipole transitions, *Astrophys. J.*, 522, 524–539, 1999.

- Gary, D. E. and Hurford, G. J.: Coronal temperature, density, and magnetic field maps of a solar active region using the Owens Valley Solar Array, *Astrophys. J.*, 420, 903–912, 1994.
- Judge, P.: Towards the measurement of coronal magnetic fields, in: *Solar Polarization 3*, edited by: Trujillo Bueno, J. and Sanchez Almeida, J., ASP Conference Series, 307, 437–445, 2003.
- Judge, P.: Spectral lines for polarization measurements of the coronal magnetic field. V. information content of magnetic dipole lines, 662, 677–690, 2007.
- Judge, P. G., Low, B. C., and Casini, R.: Spectral lines for polarization measurements of the coronal magnetic field. IV. Stokes signals in current-carrying fields, *Astrophys. J.*, 651, 1229–1237, 2006.
- Kramar, M. B., Inhester, B., and Solanki, S. K.: Vector tomography for the coronal magnetic field. I. Longitudinal Zeeman effect measurements, *Astron. Astrophys.*, 456, 665–673, 2006.
- Kramar, M. and Inhester, B.: Inversion of coronal Zeeman and Hanle observations to reconstruct the coronal magnetic field, *Memorie della Societa Astronomica Italiana*, 78, 120–125, 2007.
- Kuhn, J. R.: Infrared Coronal Magnetic Field Measurements, in: *IR Tools for Solar Astrophysics: What's Next?*, edited by: Kuhn, J. R. and Penn, M. J. (Singapore: World Scientific), p. 89–93, 1995.
- Kuhn, J. R., Coulter, R., Lin, H., and Mickey, D.: The SOLARC off-axis coronagraph, *SPIE*, 4853, 318–326, 2003.
- Lee, J., White, S. M., Kundu, M. R., et al.: A test for coronal magnetic field extrapolations, *Astrophys. J.*, 510, 413–421, 1999.
- Lin, H. and Casini, R.: A classical theory of coronal emission line polarization, *Astrophys. J.*, 542, 528–534, 2000.
- Lin, H., Penn, M. J., and Kuhn, J. R.: HeI 10830 Angstrom line polarimetry: a new tool to probe the filament magnetic fields, *Astrophys. J.*, 493, 978–995, 1998.
- Lin, H., Penn, M. J., and Tomczyk, S.: A new precise measurement of the coronal magnetic field strength, *Astrophys. J.*, 541, L83–L86, 2000.
- Lin, H., Kuhn, J. R., and Coulter, R.: Coronal Magnetic Field Measurements, *Astrophys. J.*, 613, L177–L180, 2004.
- Liu, Y. and Lin, H.: Observational test of coronal magnetic field models. I. comparison with potential field model, *Astrophys. J.*, 680, 1496–1507, 2008.
- Liu, Y. and Lin, H.: The solar coronal magnetic field measurements with SOLARC, in: *Proceedings of 10th Asian-Pacific Regional IAU Meeting 2008*, edited by: Zhang, S.-N., Li, Y., and Yu, Q., Beijing: China Science and Technology Press, p. 53–56, 2009.
- Liu, Y. and Zhang, H.: Global magnetic extrapolation based on the synoptic map of MDI/SOHO, *Publ. Yunnan Obs.*, 92, 1–9, 2002.
- Mickey, D.: Polarization Measurements in the Green Coronal Line, *Astrophys. J.*, 181, L19–L21, 1973.
- Patzold, M., Bird, M. K., Volland, H., et al.: The mean coronal magnetic field determined from HELIOS Faraday rotation measurements, *Astrophys. J.*, 109, 91–105, 1987.
- Penn, M.J., Lin, H., Tomczyk, S., Elmore, D., and Judge, P.: Background-induced measurement errors of the coronal intensity, density, velocity, and magnetic field, *Solar Phys.*, 222, 61–78, 2004.
- Querfeld, C. W.: The formation and interpretation of the FeXIII 10747 Å coronal emission line, *Astrophys. J.*, 255, 764–773, 1982.
- Querfeld, C. W. and Smartt, R. N.: Comparison of coronal emission-line structure and polarization, *Solar Phys.*, 91, 299–310, 1984.
- Stelzried, C. T., Levy, G. S., Sato, T., et al.: The quasi-stationary coronal magnetic field and electron density as determined from a Faraday rotation experiment, *Solar Phys.*, 14, 440–456, 1970.
- Tomczyk, S., McIntosh, S. W., Keil, S. L., Judge, P. G., Schad, T., Seeley, D. H., and Edmondson, J.: Alfvén waves in the solar corona, *Science*, 317, 1192–1196, 2007.
- Tomczyk, S., Card, G. L., Darnell, T., Elmore, D. F., Lull, R., Nelson, P. G., Stander, K. V., Burkepile, J., Casini, R., and Judge, P. G.: An instrument to measure coronal emission line polarization, *Solar Phys.*, 247, 411–428, 2008.
- Tomczyk, S. and McIntosh, S.: Time-distance seismology of the solar corona with CoMP, *Astrophys. J.*, 697, 1384–1391, 2009.